2023 IEEE/ASME International Conference on Advanced Intelligent Mechatronics (AIM)
June 28-30, 2023. Seattle, Washington, USA

2023 IEEE/ASME International Conference on Advanced Intelligent Mechatronics (AIM) | 978-1-6654-7633-1/23/$31.00 ©2023 IEEE | DOI: 10.1109/AIM46323.2023.10196180

Data-driven Robust Acoustic Noise Filtering for Atomic Force Microscope Image

Jiarong Chen[1] and Qingze Zou[2]

Abstract— **This paper presents a data-driven acoustic signal filtering technique to eliminate acoustic-caused distortions in atomic force microscope (AFM) image. AFM measurement is sensitive to external disturbances including acoustic signals, as disturbance to the probe-sample interaction directly results in distortions in the sample images obtained. Although conventional passive noise cancellation has been employed, limitation exists and residual noise still persists. The acoustic dynamics involved, however, is complicated, broadband, and not decaying with frequency increase. Even more challengingly, the acoustic source location being unknown and arbitrary in practice results in the signal to noise ratio (SNR) of the acoustic signal measured becomes low, and the error in the acoustic dynamics measured becomes large, both directly deteriorating the image quality obtained. In this work, we propose a Wiener-filter-based robust filtering technique to improve both the SNR of the acoustic signal measured and the error in the acoustic dynamics obtained. Then a coherence minimization approach is proposed to further enhance accuracy of the filter without modeling via a gradient-based optimization method. Experimental implementation is presented and discussed to illustrate the proposed technique.**

I. INTRODUCTION

In this paper, a data-driven dynamics-based post-filtering technique is proposed to eliminate acoustic-caused distortion in atomic force microscope (AFM) image. Based on a mechanical "touch to see" principle via a nano-size cantilever probe [4], AFM is sensitive to external disturbances including acoustic noise, as disturbances to the probe-sample interaction directly result in the distortion in AFM images [5]. Although passive noise apparatuses have been employed to combat acoustic disturbance, such a de facto industry standard faces limitations in both performance, usability and cost. Whereas active acoustic cancellation, however, is challenging, particularly when the acoustic noise is from a source at an unknown and arbitrary location. Thus, this work is motivated to tackle these challenges and develop a robust filtering approach to eliminate acoustic caused distortions in AFM image.

Maintaining the probe-sample interaction closely around the set point value is important in all AFM applications, ranging from imaging [7], [8], nanomechanical measurement, to probe-based nanofabrication. Extraneous probe vibration can be induced by both external disturbances including acoustic noise and seismic vibrations, and internal ones due to the excitement of the dynamics and hysteresis adverse effects of the nanopositioning systems (from the piezo actuator to the cantilever probe [12]). The internal adverse effects can be compensated for by increasing the bandwidth of the nanopositioning system, through hardware improvement (e.g., using piezo actuator and/or cantilever of higher bandwidth) [10], [11], and/or software enhancement of more advanced control techniques [12]. Whereas conventionally, external adverse effects are mainly accounted for through passive vibration/noise isolation apparatus [14]–[16]. Although vibration and acoustic noise effects have been mitigated, these passive apparatus are costly and bulky, not implementable for applications such as biomedical-related research where AFM needs to be integrated with other instrument like optical microscope. Moreover, residual image distortion still persists, and the image quality obtained cannot meet the stringent requirements in applications such as the cleanroom nanometrology in semi-conductor industry [17]. These acoustic-related issues have largely limited the application and impact of AFM in these and other areas. However, unlike the development of control techniques to account for internal disturbances in high-speed AFM operations [12], [13], few work has been reported on active control of acoustic noise for AFM. Recently an inversion-based feedforward controller has been introduced for online active noise control [6]. Its performance has been hurdled by the hardware constraints (e.g., online computation power and data acquisition speed) and the system bandwidth imposed by the robustness requirements. Thus, active control and/or filtering technique needs to be developed to combat acoustic noise effect on AFM image.

Challenges exist in eliminating acoustic-caused distortions in AFM image. As the noise-caused distortion is largely coupled with the sample topography in the images obtained, conventional filtering techniques based on frequency-separation (e.g., low-pass, band-pass, or notch filter) are ineffective. The acoustic-noise dynamics is highly oscillatory (i.e., contains multiple poles and zeros) and broadband, and do not decay with frequency increase, making it difficult to employ model-based approaches along with the Kalman-filtering framework [19]. This difficulty becomes even more so when the location of the noise source is arbitrary and unknown, —as usually the case in practices. The unknown and arbitrary acoustic source location can result in a low SNR in the acoustic signal measured, particularly when the

*This work was supported by the NSF grants CMMI-1851907, IIBR-1952823 and and PFI-2234449.

[1]Jiarong Chen is a graduate student in the Department of Mechanical and Aerospace Engineering, Rutgers University, Piscataway, NJ 08854, USA jiarong.chen@rutgers.edu

[2]Qingze Zou is with the Department of Mechanical and Aerospace Engineering, Rutgers University, Piscataway, NJ 08854, USA qzzou@soe.rutgers.edu

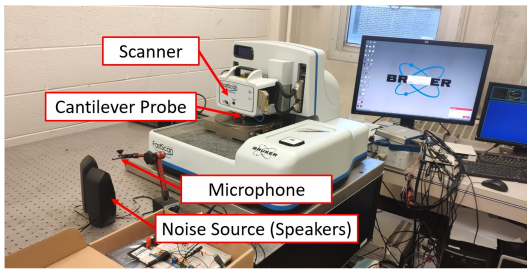

Fig. 1. An experimental setup for studying acoustic noise effect on AFM operation, where it is assumed that the location of the noise source (speakers) is unknown while the sensor (microphone) is placed at fixed and known location.

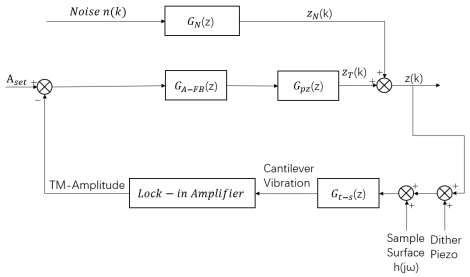

Fig. 2. Schematic block diagram of the AFM imaging process with acoustic noise

sensor (microphone) is placed distant away from the acoustic source (as practically it is unfeasible to relocate the sensor whenever the acoustic source is identified). Moreover, the unknown acoustic source also results in errors in the acoustic dynamics obtained as the acoustic dynamics depends on the noise propagation path and varies significantly as the distance and direction of the noise source changes. Thus, for the filter to be effective, the complexity of the acoustic dynamics and the unknown acoustic source location effect must be addressed.

The main contribution of this paper is the development of a data-driven robust filtering (DRF) technique to eliminate acoustic caused AFM image distortions. A Wiener filter technique is introduced to account for the adverse unknown acoustic source effect on both the acoustic signal and the acoustic dynamics measurements. Then the filters are further optimized through the coherence minimization technique [2] to maximize the SNR of the acoustic noise measured and the accuracy of the acoustic dynamics obtained. Compared to the previous work [2], the proposed approach eliminates the dictionary construction while preserving the performance. The proposed filtering scheme is implemented on AFM image examples and the experimental results show that the image distortion are significantly reduced.

II. Data-driven Acoustic Filtering of Atomic Force Microscope Image

A. Acoustic-caused AFM Image Distortions: Problem Formulation

In this work, we aim to develop an post-imaging filtering technique to eliminate the acoustic noise effect regardless the location of the acoustic source. Without loss of generality, we assume that

Assumption 1: The noise source location is fixed, arbitrary, and unknown.

Assumption 2: The acoustic noise n[k] is a zero-mean, band-limited wide-sense stationary (WSS) random process [1], and the variation of the primary acoustic noise dynamics (PAD) is quasi static.

The PAD is the dynamics from the noise signal (as the input) to the AFM image signal (as the output response) ($G_N(z)$ in Fig. 2). Assumption 2 is reasonable as the variation of the PAD is mainly caused by the change of the noise source location, i.e., the noise propagation route and the AFM configuration (e.g., mounting of the cantilever), both remain unchanged during an imaging process but can vary significantly in day to day operation.

We consider that in addition to the acoustic noise of interest (i.e., responsible for the image distortion), there also exists other measurement noise in the measured acoustic signal, such as other environmental noise and electrical thermal noise. Thus, the measured acoustic signal $n_m[k]$ measured can be generally represented as:

$$n_m[k] = n_T[k] + n_e[k] \tag{1}$$

where, respectively, $n_T[k]$ is the "true" acoustic noise causing the image distortion and $n_e[k]$ is the disturbance in the measured acoustic signal, called the acoustic measurement disturbance below.

Similarly, in the presence of the acoustic noise, the total AFM image signal $z[k]$ becomes:

$$z[k] = z_T[k] + z_n[k], \text{ for } k = 0, \cdots, N_I - 1, \tag{2}$$

where $z_{\mathrm{T}}[k]$ and $z_{\mathrm{n}}[k]$ are the z-axis piezo displacement corresponding to the sample topography and that due to the acoustic noise, and N_I is the total number of sampling data acquired in the given imaging process, respectively. As $z[k]$ is used to plot the sample topography image, in the following, $z[k]$, $z_T[k]$, and $z_n[k]$ are called the measured image signal, the true image signal, and the image noise signal, respectively.

Assumption 3: The acoustic measurement disturbance $n_e[k]$ is a zero-mean, wide-sense stationary (WSS) random process, uncorrelated to both the acoustic noise $n_T[k]$ and the measured image signal $z[k]$.

Thus, the filtered image signal, $z_F[\cdot]$, can be obtained from the image noise signal, $\hat{z}_n[k]$, via

$$z_F[k] = z[k] - \hat{z}_n[k], \text{ for } k = 0, \cdots, N_I - 1, \tag{3}$$

and the filtering quality can be quantified by the residual image error $e[k]$

$$e_r[k] = z_T[k] - z_F[k]. \tag{4}$$

Data-driven Robust Filtering (DRF) of Acoustic-caused AFM Image Distortion Let Assumptions 1-3 hold, the

DRF problem is to design a filter directly from the measured acoustic noise and the AFM image signals (without a parameterized model), such that

$\mathbb{O}$-1 The estimated acoustic noise $\hat{n}\dagger[k]$ is also a zero-mean WSS, and the SNR of the measured acoustic signal is optimized the variance of the acoustic noise estimation error,

$$\min_{\hat{n}[k]} J_n = \mathbf{E}\{n_T[k] - \hat{n}[k]\}^2, \tag{5}$$

$\mathbb{O}$-2 The filter $\hat{g}_N^{\dagger}[k]$ is constructed by using the measured data directly such that the expectation of the error between the true image and the filtered image is zero,

$$\mathbf{E}(e[k]) = \mathbf{E}\{z_T[k] - z_F[k]\} = 0 \tag{6}$$

and the variance of the error is minimized.

$$\min_{\hat{g}_n[k]} J_z = \mathbf{E}\{e[k]\}^2 \tag{7}$$

We proceed by achieving the two objectives in order.

B. [$\mathbb{O}$-1] Optimal Acoustic Signal Estimation: Wiener Filter Approach

We propose to optimize the estimation of the acoustic noise signal $\hat{n}^{\dagger}[\cdot]$ in Eq. (5) via the Wiener filter approach [1]. The key idea is to estimate the acoustic noise signal $\hat{n}[k]$ by replacing the noise-caused displacement by the measured z-axis displacement, i.e., the image signal instead via

$$\hat{n}[k] = \hat{g}_z[k] * z[k] \tag{8}$$

where $\hat{g}_z[k]$ is an estimation of the inverse dynamic from noise to z-axis displacement $g_z[k]$. An optimal filter $\hat{g}_z^{\dagger}[k]$ can be sought by minimizing the square of the correlation between the following estimated acoustic measurement disturbance $\hat{n}_e[k]$ below

$$\hat{n}_e[k] = n_m[k] - \hat{n}[k] \tag{9}$$

and the measured image signal $z[k]$,

$$\min_{\hat{g}_n[k]} r_{nz}^2[j] = \mathbf{E}\{\hat{n}_e[k]z[k-j]\}^2, \tag{10}$$

It can be shown that under the given conditions (Assumptions 1-3), an accurate estimation of the "true" acoustic noise signal $n_T[k]$, $\hat{n}[k]$, can be obtained by minimizing the correlation in Eq. (10).

The cost function in Eq.(10) can be further rewritten by using Eq. (9) as

$$J_m = \mathbf{E}\{\mathbf{p} - \mathbf{R}\mathbf{g}_\mathbf{z}\}^2 \tag{11}$$

where $\mathbf{p}$ is the cross-correlation between the measured acoustic noise $n_m[k]$ and $z[k]$,

$$\mathbf{p} = \mathbf{E}\{\mathbf{n_m}(k)\mathbf{z^T}(k)\} = [p(0)\ p(-1)\ \cdots\ p(-N_F+1)]^T \tag{12}$$

The auto-correlation matrix of measured image signal $z[k]$, $\mathbf{R}$ is given by

$$\mathbf{R} = \mathbf{E}\{\mathbf{z}(k)\mathbf{z}^T(k)\} \tag{13}$$
$$= \begin{bmatrix} R[0] & R[1] & \dots & R[N_F-1] \\ R[1] & R[0] & \dots & R[N_F-2] \\ \vdots & \vdots & \ddots & \vdots \\ R[N_F-1] & R[N_F-2] & \dots & R[0] \end{bmatrix}$$

thus the optimal filter weight of $g_z[k]$ can be readily obtained as a Wiener filter [1] via the minimization of the cost function in Eq. (11)

$$\mathbf{g}_z^{\sharp} = \mathbf{R}^{-1}\mathbf{p} \tag{14}$$

As both $n_e[k]$ and $n_m[k]$ are wide-sense stationary processes , the auto-correlation matrix $\mathbf{R}$ is nonsingular for any non-zero measurement disturbance $n_e[k]$ [1]. Therefore, the estimated acoustic measurement disturbance is obtained as

$$\hat{n}^{\sharp}[k] = \mathbf{g}_z^{\sharp} * z[k], \tag{15}$$

i.e., the acoustic noise $n_T[k]$ is estimated by using the auto-correlation of the noise-effected image modulated by the cross-correlation with the measured acoustic signal.

Steepest Descent Method to Compute the Wiener Filter Finding the Wiener filter can be computationally costly when the related acoustic dynamics is complicated and the order of the FIR filter N_F increases. Thus, we utilize the steepest descent method [1] to seek the optimal $g_z[k]^{\dagger}$ via the following recursive iteration

$$\mathbf{g}_{z,i+1} = \mathbf{g}_{z,i} + \mu\mathbf{E}\{\mathbf{z}_i(k)\hat{n}_e(k)\} \tag{16}$$

where

$$\mathbf{z}_i = [z[k+i]\ z[k-1+i]\ \cdots\ z[k-N_F+1+i]]^T \tag{17}$$

and initially

$$\mathbf{g}_{z,0} = \mathbf{0} \tag{18}$$

The exact value of the correlation between the raw image signal and estimated acoustic measurement disturbance $\mathbf{z}_i[k]\hat{n}_e(k)$ is unknown, in general. The following estimation is employed by using the values of the two signals at current sampling instant,

$$\mathbf{E}\{\mathbf{z}_i(k)\hat{n}_e(k)\} \approx \mathbf{z}_i(k)\hat{n}_e(k) \tag{19}$$

The step size μ is chosen to ensure the convergence of the recursive iteration in Eq. (16).

Modulator-based Filter Optimization The estimation Eq. (19) introduces errors into the steepest descent method. Such an estimation error can be utilized to further enhance the noise measurement filter $\hat{g}_z[\cdot]$. We introduce a frequency domain modulator to further enhance the disturbance noise filter $\hat{g}_z[\cdot]$ in frequency domain, as in

$$\hat{G}_z^{\dagger}(e^{j\omega_k}) = \alpha_{\dagger}(e^{j\omega_k})G_z^{\sharp}(e^{j\omega_k}) \tag{20}$$

where $G_z(e^{j\omega})$ denotes the z-transform of the noise measurement filter $\hat{g}_z[\cdot]$, $\omega_k = \frac{k\omega_s}{N_I}\ for\ k = 0, 1, \cdots, N_I -$

1 *and* $\omega_s = 2\pi f_s$ are the discrete sampled frequencies, such that the coherence between the estimated measurement disturbance $\hat{n}_e^\sharp[k]$ and the measured image signal $z[k]$ is minimized, i.e., find $\alpha_\dagger(e^{j\omega_k})$ such that the coherence between $\hat{n}_e^\sharp[k]$ and $z[k]$

$$\min \ \mathbf{C}_{nz}(e^{j\omega_k}) = \frac{\mathbf{E}[\hat{N}_e^*(e^{j\omega_k})Z(e^{j\omega_k})]^2}{\hat{P}_{N_e}(e^{j\omega_k})P_Z(e^{j\omega_k})} \tag{21}$$

is minimized.

It can be shown that under the given conditions (Assumptions 1-3), the acoustic disturbance estimation filter $g_z^\dagger[k]$ that minimizes the cost function Eq.(5) can be obtained through the minimization of the coherence $\mathbf{C}_{nz}(e^{j\omega_k})$ in Eq. (21).

We propose a gradient-based iterative descend method [2] to search the optimal $\alpha^\dagger(e^{j\omega_k})$ to minimize cost function Eq. (21). This has been developed recently in [2], and the readers are referred to Ref. [2] for more details. Hence, the estimated acoustic noise is given as

$$\hat{n}^\dagger[k] = \mathbf{g}_z^\dagger * z[k], \tag{22}$$

C. [𝕆-2] Optimal acoustic-noise Filter Design

We propose a modulator-based acoustic filter $\hat{G}_n^\dagger(e^{j\omega_k})$ to minimize the cost function Eq. (6) as in Ref. [2]

$$\hat{G}_n^\dagger(e^{j\omega_k}) = \beta_\dagger(e^{j\omega_k})G_n(e^{j\omega_k}) \tag{23}$$

where the filter $G_n(e^{j\omega_k})$ is based on the PAD and can be experimentally acquired, and $\beta_\dagger(e^{j\omega_k})$ is the frequency-dependent modulator, respectively. The filter $G_n(e^{j\omega_k})$, is obtained experimentally a priori, by acquiring the image signal under a fixed-location acoustics excitation $Z_{WN}(e^{j\omega_k})$ when the cantilever tip is engaged onto the sample without scanning, and a band-limited white noise acoustic noise $N_{WN}(e^{j\omega_k})$ is broadcasted to the environment

$$G_n(e^{j\omega_k}) = \frac{Z_{WN}(e^{j\omega_k})}{N_{WN}(e^{j\omega_k})} \tag{24}$$

and the optimal modulator $\beta_\dagger(e^{j\omega_k})$ is obtained by minimizing the following coherence between $n^\dagger[k]$ and filtered image $z_F[k]$,

$$\min \mathbf{C}_{nf}(e^{j\omega_k}) = \frac{\mathbf{E}[N^*(e^{j\omega_k})Z_F(e^{j\omega_k})]^2}{P_N(e^{j\omega_k})P_{Z_F}(e^{j\omega_k})} \tag{25}$$

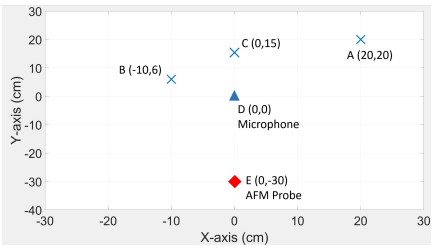

Fig. 3. The location of the acoustic noise source placed at three "unknown" location respect to the microphone and the AFM probe, respectively.

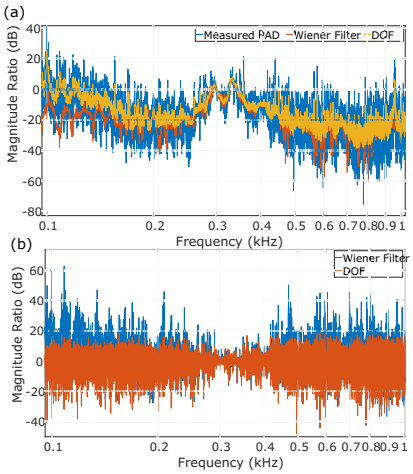

Fig. 4. (a) Frequency response (magnitude part) of the measured PAD and those estimated by using the Wiener filter and the the Data-Driven Robust Filtering (DRF) method and (b) the error (magnitude part) of the estimated dynamics of Wiener Filter, and that of the DRF method compared to the measured PAD, respectively.

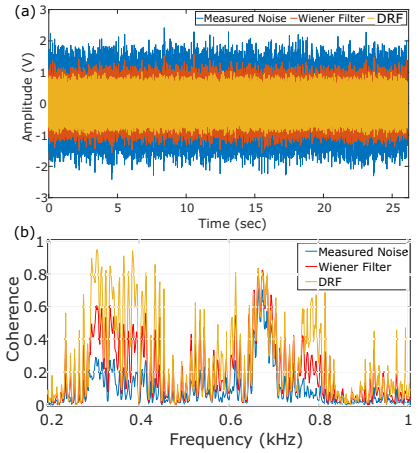

Fig. 5. (a) Measured acoustic noise signal of low SNR compared to the filtered noise by Wiener Filter and DRF method, and (b) the coherence between the z-axis displacement to the measured noise, noise filtered by Wiener Filter compared to the noise filtered by DRF, respectively.

It can be shown that such a filter $\hat{G}_n^\dagger(e^{j\omega_k})$ accounts for the uncertainty and variations in the PAD caused by the unknown noise location and the non-collocation of the acoustic source and the sensor (microphone), thereby, minimizes the cost function Eq. (6). As such, the dictionary of PAD and Noise Propagation Dynamic (NPD) employed previously in [2] can be omitted without loss of performance and robustness. The gradient-based iterative descend method is employed to search the optimal $\beta^\dagger(e^{j\omega_k})$ that minimizes cost function Eq. (25), i.e., seek $\beta(e^{j\omega_k})$ to minimize the estimated coherence $C_{nf}(e^{j\omega_k})$.

III. Experiment Example

The proposed approach was demonstrated through an AFM imaging experiment. The AFM imaging experiment was performed on a commercial AFM system (Dimension FastScan, Bruker Nano Inc.), where the acoustic noise was

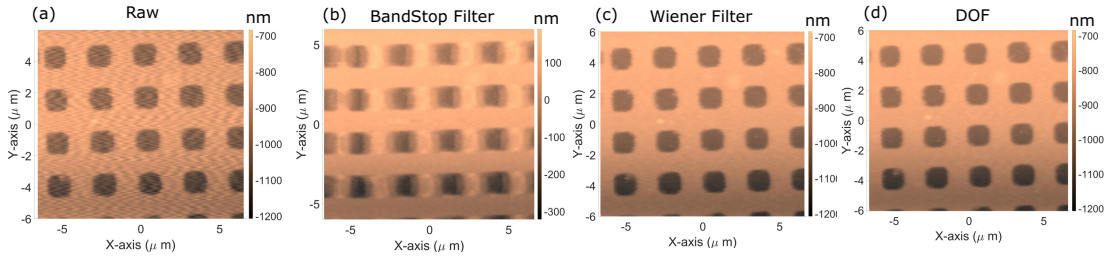

Fig. 6. Comparison of the original raw image of a calibration sample obtained at a scan rate of 5 Hz (a) under the induced acoustic noise, and those filtered by (b) a bandstop filter, and (c) Wiener Filtering and (d) the DRF filtering, respectively.

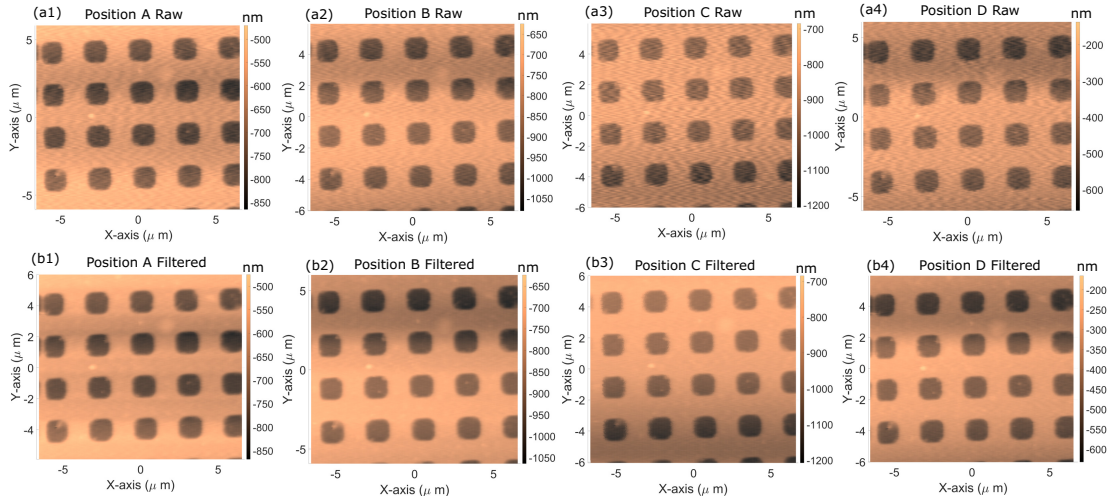

Fig. 10. Comparison of the raw image of the calibration sample obtained at a scan rate of 5 Hz top row, (a1-a4) under the induced acoustic noise to those bottom row (b1-b4) filtered by using the DRF technique at three different locations, respectively, where (a4) and (b4) (Position D) shows the result with the noise source and the microphone is collocated.

induced by a speaker placed near the AFM scanner head, and measured via a precision array microphone (BK 4958, Bruel Kjaer Inc.), as shown in Fig. 1. The ground vibration effect induced by the speaker on the cantilever probe vibration became part of the PAD of the setup, therefore, was accounted for in the proposed approach. The noise sensor signal was first pre-filtered and amplified using a homemade Op-Amp circuit, and then measured via a data acquisition system (NI RIO, USB-7856R, National Instrument Inc.). All the filtering algorithms were designed and implemented in MATLAB (Mathworks Inc.).

Experimental Implementation

First, the acoustic-noise-effected AFM images were acquired under the acoustic noise effect from a noise source at three different "unknown" locations with the sensor (microphone) placed at a fixed location (as shown in Fig. 3). A calibration sample (STR-1800R) was imaged at a scan rate of 5 Hz under tapping mode when a band-limited (20-1kHz) white noise with zero-mean and constant variance of 100 dB was boardcasted to the room through the speaker at one "unknown" location A (see Fig. 3), while the microphone was placed at a known and fixed location (location "D" in Fig. 3) that was 28 cm distant away from the noise source. Such an imaging process was repeated twice by placing the speaker at two other "unknown" locations (locations "B" and "C" in Fig. 3), respectively. Both the noise signals and the z-axis piezo displacements were acquired simultaneously during the imaging processes. Then, to filter the acoustic noise from location "A", the Wiener filter for filtering of the measured acoustic noise (to improve its SNR) $g_z[k]$ and for filtering sample topography $g_n[k]$ were constructed using the PAD from the measured noise signal $n_m[k]$ and raw image signal $z[k]$. Next, both filters were further optimized by the modulator-based coherence minimization method (described in Sec. 2). Finally, the filtered images were obtained by using both optimized filters to obtain the filtered image. The same procedure was repeated for filtering the images captured at the other two unknown locations B and C. For comparison, the images are also filtered directly by using the Wiener filter-based filter $g_z^\sharp[k]$ and $g_n^\sharp[k]$. Finally, the images were filtered by using a bandstop filter with the cutoff frequency range of 250 to 400 Hz. The images obtained by using the directly measured noise and DRF were presented for comparison.

Experimental Results and Discussion

The experimental results are shown in Figs. (4)-(7). The filtered location-"A" acoustic signal via the proposed Wiener filter and the DRF method, $\hat{n}[\cdot]$, were used to quantify the PAD and compared to that quantified by using the measured

signal (without filtering) directly in Fig. 4. Also, the PAD was also quantified under the sensor-speaker collocation condition, and then used as reference, as shown in fig. 4 (b). Also, the original measured noise signal is compared to the filtered noise signal by using the Wiener filter and the DRF method in Fig. 5 for location "A". The raw acoustic-effect image of the calibration sample is compared to those filtered by using the bandstop filter, the Wiener filter and the DRF filter in Fig. 6, respectively. Then, the filtering results of the proposed DRF technique for the images captured at the three unknown speaker locations are shown Fig. 7. The imaging results demonstrated that the distortion caused by acoustic noise from an arbitrary unknown location can be substantially reduced by using the proposed approach. First, the Wiener filter captured the measured PAD well, with most of the poles and zeros of the Wiener filter overlapped with those of the measured PAD well (see Fig. 4 (a)). The error of PAD was significantly further reduced by using the proposed DRF filter as shown in Fig. 4(b). Next, the SNR of the measured acoustic noise signal was significantly improved by using the Wiener filter as more than 50 % of the irrelevant noise was removed from the signal and another 10% was reduced by DOF. Such an improvement in the SNR resulted in the elimination of the acoustic-caused image distortion while maintaining the sample topography features. As shown in Fig. 6 (c), by using the Wiener filter, the acoustic-caused image distortion was largely removed, whereas when using the bandstop filter, the edge of the pitches were severely smeared in the filtered image (see Fig. 6 (b)). However, by using the proposed DRF filter, the image quality was further improved (see Fig. 6 (d)). To be specific, the relative 2-norm error was reduced by 68% by using the Wiener-filter-based filter, and then further by another 10% by using the proposed DRF filter. Finally, the experimental results also demonstrated the proposed DRF filter is robust against the variation of the noise source location. As shown in Fig. 7, the 2-norm image error at three different locations are consistent between 14% to 19% and compared well to the 13% image error under the condition that the noise source and microphone collocated. Therefore, the experimental results demonstrated the efficacy of the proposed approach.

IV. Conclusion

A data-driven robust-optimal filtering technique was developed to eliminate AFM image distortion caused by acoustic noise. The Wiener filter in the FIR representation is explored to construct the filter and improve the SNR of the measured acoustic signal. It is shown that by introducing a modulator into the filters, the error in the estimated acoustic dynamics and the low SNR of the measured acoustic noise can be eliminated by optimizing the modulator via a gradient-based coherence minimization approach. The efficacy of the proposed approach was demonstrated by filtering experimentally measured AFM images. The results showed that the image distortion was substantially reduced by the proposed technique.

References

[1] S. S. Haykin Adaptive filter theory[M]. Pearson Education India, 2013.

[2] J. Chen, Q. Zou Data-driven dynamics-based optimal filtering of acoustic noise at arbitrary location in atomic force microscope imaging[J]. Ultramicroscopy, 2022, 242: 113614.

[3] P. Welch, "The use of fast Fourier transform for the estimation of power spectra: A method based on time averaging over short, modified periodograms" in IEEE Transactions on Audio and Electroacoustics, vol. 15, no. 2, pp. 70-73, June 1967, doi: 10.1109/TAU.1967.1161901.

[4] M. Gruber (1997) *Statistical Digital Signal Processing and Modeling*, Technometrics,39:3, 335-336

[5] F. Gołek, P.Mazur, Z.Ryszka, S.Zuber, "AFM image artifacts". Applied Surface Science, 304, June, 2014 pp. 11–19, https://doi.org/10.1016/j.apsusc.2014.01.149

[6] S. Yi, T. Li, Q. Zou, "Active control of acoustics-caused nano-vibration in atomic force microscope imaging". Ultramicroscopy, 195, December 2018, pp. 101–110, https://doi.org/10.1016/j.ultramic.2018.07.006

[7] J. Ren, Q. Zou, "Adaptive-scanning, near-minimum-deformation atomic force microscope imaging of soft sample in liquid: Live mammalian cell example", Ultramicroscopy, Volume 186, 2018, Pages 150-157, ISSN 0304-3991, https://doi.org/10.1016/j.ultramic.2017.12.020.

[8] T. Uchihashi, H. Watanabe, S. Fukuda, M. Shibata, T. Ando, "Functional extension of high-speed AFM for wider biological applications", Ultramicroscopy, Volume 160, 2016, Pages 182-196, https://doi.org/10.1016/j.ultramic.2015.10.017.

[9] H. Xie and S. Régnier, "High-Efficiency Automated Nanomanipulation With Parallel Imaging/Manipulation Force Microscopy" in IEEE Transactions on Nanotechnology, vol. 11, no. 1, pp. 21-33, Jan. 2012, doi: 10.1109/TNANO.2010.2041359.

[10] G. Schitter, K. J. Astrom, B. E. DeMartini, P. J. Thurner, K. L. Turner and P. K. Hansma, "Design and Modeling of a High-Speed AFM-Scanner" in IEEE Transactions on Control Systems Technology, vol. 15, no. 5, pp. 906-915, Sept. 2007, doi: 10.1109/TCST.2007.902953.

[11] T. Ando, T. Uchihashi, N. Kodera, et al, "High-speed AFM and nano-visualization of biomolecular processes", Pflugers Arch - Eur J Physiol 456, 211–225 (2008). https://doi.org/10.1007/s00424-007-0406-0

[12] G. M. Clayton, S. Tien, K. K. Leang, Q. Zou, and S. Devasia, (October 28, 2009), "A Review of Feedforward Control Approaches in Nanopositioning for High-Speed SPM." ASME. J. Dyn. Sys., Meas., Control. November 2009; 131(6): 061101. https://doi.org/10.1115/1.4000158

[13] A. Sebastian, A. Gannepalli, & M. V. Salapaka, (2007) A review of the systems approach to the analysis of dynamic-mode atomic force microscopy. IEEE Transactions on Control Systems Technology, 15(5), 952-959.

[14] W. Zhang, G. Meng and Z. Peng, "Nonlinear Dynamic Analysis of Atomic Force Microscopy Under Bounded Noise Parametric Excitation" in IEEE/ASME Transactions on Mechatronics, vol. 16, no. 6, pp. 1063-1072, Dec. 2011, doi: 10.1109/TMECH.2010.2073715.

[15] S. Ito, D. Neyer, S. Pirker, J. Steininger and G. Schitter, "Atomic force microscopy using voice coil actuators for vibration isolation" 2015 IEEE International Conference on Advanced Intelligent Mechatronics (AIM), 2015, pp. 470-475, doi: 10.1109/AIM.2015.7222578.

[16] F. Benmouna, D. Johannsmann, "Hydrodynamic interaction of AFM cantilevers with solid walls: An investigation based on AFM noise analysis", Eur. Phys. J. E 9, 435–441 (2002). https://doi.org/10.1140/epje/i2002-10096-x

[17] Ducourtieux, S., & Poyet, B. (2011). Development of a metrological atomic force microscope with minimized Abbe error and differential interferometer-based real-time position control. Measurement Science and Technology, 22(9), 094010.

[18] N. Gadegaard (2006) "Atomic force microscopy in biology: technology and techniques", Biotechnic & Histochemistry, 81:2-3, 87-97, DOI: 10.1080/10520290600783143

[19] M. G. Ruppert, K. S. Karvinen, S. L. Wiggins and S. O. Reza Moheimani, "A Kalman Filter for Amplitude Estimation in High-Speed Dynamic Mode Atomic Force Microscopy" in IEEE Transactions on Control Systems Technology, vol. 24, no. 1, pp. 276-284, Jan. 2016, doi: 10.1109/TCST.2015.2435654.